Engenharia Agrícola
ISSN: 1809-4430 (online)
www.engenhariaagricola.org.br | www.scielo.br/j/eagri

Scientific Paper
DOI: http://dx.doi.org/10.1590/1809-4430-Eng.Agric.v45e20240115/2025

DESIGN AND TEST OF A SUPPORT CUTTING ANTI-CLOGGING DEVICE WITH VIBRATION FOR A NO-TILL SEEDER

Mengnan Yin[1], Wenjun Wang[1*,2,3], Yulong Chen[1,2,3], Long Zhou[1,2,3], Mingwei Li[1,2,3]

[1*]Corresponding author. School of Agricultural Engineering and Food Science, Shandong University of Technology, Zibo, China. E-mail: wjwang2016@163.com | ORCID ID: https://orcid.org/0000-0001-7101-3763

KEYWORDS

agricultural machinery, no-till seeder, stubble breaking, anti-clogging mechanism, vibrating knife.

ABSTRACT

The anti-clogging device of a no-till seeder is an important component that affects the seeding quality. In one year two crop area of China, a no-tillage seeder for corn generally includes a passive anti-clogging device, and there are often problems with straw winding around working parts due to the low straw cleaning rate. To solve these problems, a support cutting anti-clogging device with vibration for a no-till seeder was designed in this study to efficiently cut wheat stalks and remove them to the sides of the seedbed. Through theoretical calculations and kinematic analysis, the main structural parameters of the device were limited to small ranges of values: the mounting angle of the vibrating knife was in the range θ_1 = 70–82°, the amplification was in the range l_1 = 14–24 mm, and the frequency was in the range ω_m = 240–340 rad/min. To analyse the effects of the main parameters on the average straw cutting rate, soil bin experiments were carried out using an orthogonal multinomial regressive experimental design with three factors and three levels. The optimal structural parameters derived in this way were as follows: mounting angle for the vibrating knife θ_1 = 70.7°, amplification l_1 = 19 mm, and frequency ω_m = 330.2 rad/min. The results of adaptability and comparison tests showed that the average straw cutting rate was 93.30% when the proposed anti-clogging device with vibration was used. Compared to traditional devices, the cutting rate for the device was increased by 12.82%, and the metrics were superior to those of a traditional anti-clogging device. This research can serve as a reference for designing anti-clogging devices for no-till seeders.

INTRODUCTION

With the continuous developments in the area of modern agricultural technology, the designs of anti-clogging devices for no-till seeders have become more diverse. Huang et al. (2020) reported that the anti-clogging device for a corn no-tillage seeder is prone to several problems during operation, and to solve these, the device needs to be redesigned to give a better straw cutting rate and higher performance stability.

Scholars around the world have classified commonly used anti-clogging devices into two types: passive and active. As a passive anti-clogging device, Liu et al. (2018) designed a grass separation device with a driven rotating tooth disc, which solved the problems of the high power consumption and complex structure of traditional anti-clogging devices. Fan et al. (2011) designed a finger-type anti-clogging residue-cleaner for no-till planting; the working principle of this machine was based on a star wheel, which could reduce the wheat straw stubble cover and bare soil. Zhu et al. (2023), at the Fleischer Manufacturing Company, used a working principle based on a crushing mechanism, with a device consisting of a cutting wheel and a depth-limiting wheel. Hong (2021) used a double-disc opener trencher for trenching, in which the disc furrower for the seeder was equipped with grass teeth, which facilitated the movement of straw towards both sides of the trencher. The passive anti-clogging devices discussed above are simple to install. However, they have low cutting rates and are susceptible to clogging at high speeds.

[1] School of Agricultural Engineering and Food Science, Shandong University of Technology, Zibo, China.
[2] Institute of Modern Agricultural Equipment, Shandong University of Technology, Zibo, China.
[3] Shandong Provincial Key Laboratory of Intelligent Agricultural Technology and Intelligent Agricultural Machinery Equipment for Field Crops, Zibo, China.

Area Editor: Geice Paula Villibor
Received in: 7-2-2024
Accepted in: 11-27-2024

In the area of active devices, Yao et al. (2020) developed an anti-clogging device for strip-to-row active corn no-tillage seeding in which the knife layout structure and cutter shaft speed were optimised. This approach was able to solve the problems of frequent blockage of the opener and poor sowing quality. Zhu et al. (2023) designed a bionic shifting and diffluence straw anti-clogging device, and found that the navigability of the device was increased by exposing its anti-clogging mechanism. Zhang et al. (2017) developed a rotary combination rice seeder that performed multiple functions in a single operation: rotary ploughing, stubble management, anti-blocking, deep fertiliser application, wide seedling belt seeding, mulching, and suppression. Fallahi & Raoufat (2007) used straw mulch in their study, and evaluated the effectiveness of a combined anti-clogging device. Their findings indicated that the combined anti-clogging device could be effectively adapted to this context. Li et al. (2022) pointed out that the existing active anti-clogging devices can overcome some of the aforementioned issues, their effectiveness is limited by their complex structures and high power consumption. To address these challenges, a support cutting anti-clogging device with vibration was specifically developed for a no-till seeder in this study. The aims of the device were to enhance the efficiency of wheat straw cutting and to effectively move straw to the peripheries of the seedbed.

MATERIAL AND METHODS

Structure and working principle of the proposed anti-clogging device with vibration

Structure of the device

The structural components of the proposed support cutting anti-clogging device with vibration are illustrated in Fig. 1, and include a stepping motor, notched disc, vibrating knife, frame, connecting rod, eccentric wheel, and straw clearing wheel. The notched disc is designed to enter the soil to a depth of 50 mm, while the straw clearing wheel has a working width of 220 mm. The edge of the notched disc cutter is designed in the form of an Archimedes spiral, which improves the cutting efficiency, reduces energy consumption, and prevents entanglement of the wheat straw. Another advantage is that this single-sided open edge design reduces the cutting resistance. The crank linkage mechanism uses power from the stepping motor to drive the vibrating knife, and the angle and amplitude are controlled by adjusting the connection position of the connecting rod ends. This adjustment changes the flexibility of the vibrating knife and improves the wheat straw cutting process. The cutting portion of the vibrating knife also employs a single-sided cutting edge, which is paired with the notched disc to facilitate a supported cutting action. The straw clearing wheel moves straw and weeds to both sides of the seedling belt, thereby enhancing the quality of sowing and crop yield.

In summary, this paper presents a support cutting anti-clogging device with vibration for a no-till seeder, which is designed to reduce cutting resistance, enable rapid cutting, decrease energy consumption, and improve work quality.

Working principle of the device

The device is attached to the seeder monomer by means of bolts and nuts on the fixing plate at the end of the frame. As the seeder advances, the blade of the notched disc exerts pressure on the soil surface, causing wheat straw and weeds to be cut off. At the same time, the eccentric wheel is driven to rotate by the stepping motor, and the vibrating knife receives power from the connecting rod to complete the reciprocating cutting movement. Subsequently, the vibrating knife and the notched disc perform vibratory cutting, and the wheat straw and weeds below the notched disk are cut off. The frequency and amplitude of the vibrating knife can be changed by adjusting the speed of the stepper motor and the positions of the ends of the connecting rod. Finally, the straw clearing wheel clears the straw and weeds to the sides.

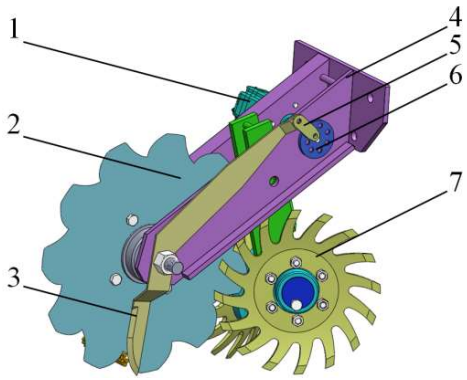

FIGURE 1. Proposed support cutting anti-clogging device with vibration for a no-till seeder:
1: stepping motor, 2: notched disc, 3: vibrating knife, 4: frame, 5: connecting rod, 6: eccentric wheel, 7: straw clearing wheel

Design of the support cutting anti-clogging device with vibration

Design of the notched disc

Cutting off the surface wheat straw is very important in terms of the efficiency of the machine. A force analysis of the notched disc is shown in Fig. 2.

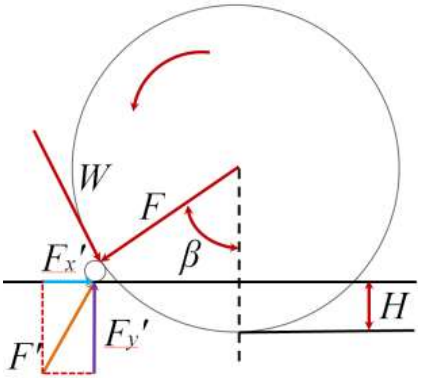

FIGURE 2. Forces on the notched disc and straw

From the figure, it can be seen that the condition of the straw not dragging on the pile is given by eqs (1) and (2).

$$\begin{cases} F_y' = F\cos\beta + W\sin\beta \\ F_x' + F_y'\cos\beta \geq F\sin\beta \end{cases} \quad (1)$$

Where:

F is the force exerted on the straw by the notched disc;

W is the friction force between the notched disc and the straw;

F' is the force between the ground and the straw;

Fx' is the horizontal component of the force;

Fy' is the vertical component of the force;

β is the angle between the force exerted by the notched disc on the straw and the vertical direction.

$$\begin{cases} \cos\beta = 1 - \dfrac{2H+d}{D} \\ F_x' = F_y'\tan\eta_1 \\ W = F\tan\eta_2 \\ \beta \leq \eta_1 + \eta_2 \end{cases} \quad (2)$$

Where:

H is the soil cutting depth of the notched disc;

D is the diameter of the notched disc;

d is the diameter of the straw;

η_1' is the friction angle between the straw and the ground;

η_2' is the friction angle between the straw and the notched disc.

Combining the above equations yields [eq. (3)]:

$$arc\cos\left(1 - \frac{2H+d}{D}\right) \leq \eta_1 + \eta_2 \quad (3)$$

To create optimal seedbed conditions, it is essential that the notched disc penetrates the root node of the straw, and the optimal depth for the notched disc was therefore set to 50 mm. Yao et al. (2022) concluded that the optimal friction angle between the straw and the ground was $\eta_1 = 30°$, while the optimal friction angle between the straw and the notched disc was $\eta_2 = 28°$. It was also determined that the diameter range of the notched disk was $D > 382$ mm. In this paper, a disc milling cutter with a diameter of 400 mm was chosen based on structural considerations of the frame.

Designing the blade curve of the notched disc according to the contact process with straw can significantly influence the power consumption and efficiency of the cutter. After an analysis of the contact process, the curve of the notched disc blade was segmented into two sections, AB and BC. Section AB was defined as the soil entry section; it was designed to reduce the resistance of the notched disk when entering the soil, hence ensuring optimum milling results. BC is the cutting section, which is fundamental to the design of the notched disc and has an impact on the cutting power consumption. In the working process of the notched disc, any point at which straw is cut is taken as the research object, as illustrated in Fig. 3(a).

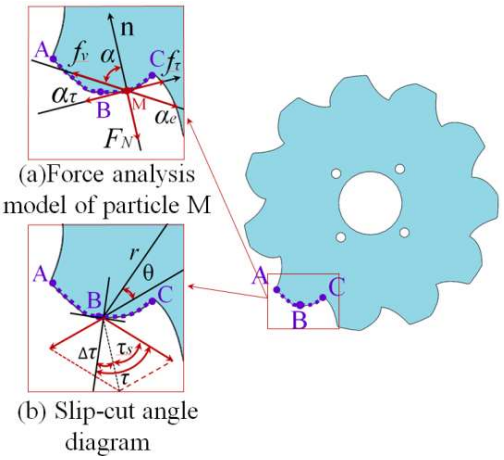

FIGURE 3. Analysis of the forces on the cutting edge of the notched disc.

An analysis was conducted in both the tangential and normal directions of the edge to derive the equations for the point in these directions, as expressed in eqs (4)–(6):

$$F_N - f_v\cos\alpha = m_1 a_e\cos\alpha \quad (4)$$

$$f_v\sin\alpha - f_\tau = m_1\left(a_\tau - a_e\sin\alpha\right) \quad (5)$$

$$f_\tau = F_N\tan\varphi \quad (6)$$

Where:

F_N is the normal pressure on the cutter edge;

f_v is the friction force in the direction of motion;

α is the cutting sliding angle;

m_1 is the mass of particle M;

α_e is the implicate the acceleration;

f_τ is the frictional force in the tangential direction;

α_τ is the acceleration in the tangential direction to the cutter edge;

φ is the frictional angle.

Equation (7) can be obtained by inserting [eq. (6)] into eqs (4) and (5):

$$F_N(\tan\alpha - \tan\varphi) = ma_\tau \quad (7)$$

As shown in Fig. 3(b), the condition for the existence of relative motion and slip shear at the contact point is $\alpha > \varphi$ (Bi et al. (2020)). The polar equation of the eccentric arc curve can be calculated by [eq. (8)]:

$$r^2 - 2re\cos\theta + e^2 = R_1^2 \tag{8}$$

Where:

e is the eccentricity;

R_1 is the radius of the eccentric circle.

The ratio of R_1 to e can be set to E to obtain [eq. (9)]:

$$r = e\cos\theta + e\sqrt{E^2 - sin^2\theta} \tag{9}$$

The static cutting sliding angle can then be calculated using the following eqs (10)–(12):

$$\tau = arc\frac{r}{\frac{dr}{d\theta}} = arc\tan\left(-\frac{\sqrt{E^2 - sin^2\theta}}{sin\theta}\right) \tag{10}$$

$$\Delta\tau = arc\tan\frac{R\cos\theta}{r - R\sin\theta} \tag{11}$$

$$\Delta\tau = \tau - \tau_s \tag{12}$$

The dynamic cutting sliding angle can also be determined using [eq. (13)]:

$$\tau_s = \arctan\left(-\frac{\sqrt{E^2 - \sin\theta}}{\sin\theta}\right) - arctan\frac{R\cos\theta}{r - R\sin\theta} \tag{13}$$

Equation (13) indicates that the dynamic cutting sliding angle τ_s depends on the radius and eccentricity of the eccentric circle. Zhao et al. (2018) concluded that the ratio of R_1 to e should be taken as 1.25, with a radius of the eccentric circle of R_1 = 125 mm, and a value for the eccentricity of e = 100 mm. The dynamic cutting slide angle is τ_s = 36–49°, as shown in [eq. (13)].

Design of the vibrating knife

When the Archimedes spiral is used as an edge curve, it has the advantages of efficient cutting and reduced wear, and this type of curve was therefore chosen for the vibrating knife. A force analysis was carried out on the straw as shown in Fig. 4.

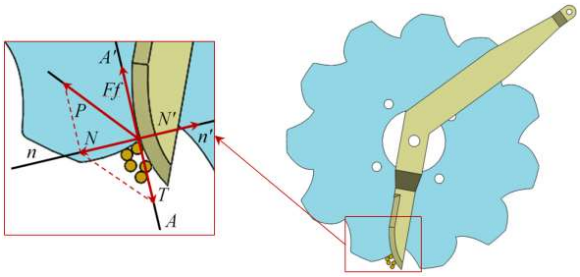

FIGURE 4. Schematic diagram of the cutting process of the vibrating knife

The straw cross-section is regarded as a mass point p, to which the vibrating knife is applied along the blade tangent direction A-A′. Liao et al. (2023) stated that the condition for the vibrating knife to produce a slip-cutting action on the straw is $T > F_f$, and the force equation for straw can then be obtained as given in [eq. (14)]:

$$\begin{cases} T = N\tan\tau_C \\ F_f = \mu N \\ \mu = \tan\eta_3 \end{cases} \tag{14}$$

Where:

N is the normal reaction force at the edge of the vibrating knife;

T is the component of N in the direction tangential to the cutter edge;

P is the component of N in the direction tangential to the motion trajectory;

N' is the normal reaction force under the combined force of the soil and the notched disc;

F_f is the friction in the tangential direction at the edge of the vibrating knife;

τ_c is the dynamic cutting sliding angle at the point of action of the vibrating knife;

μ is the coefficient of friction between the vibrating knife and the straw;

η_3 is the friction angle between the vibrating knife and the straw.

As can be seen from [eq. (14)], when $\tau_c > \eta_3$, the vibrating knife exerts a sliding cutting effect on the straw. Chen et al. (2016) concluded that a suitable range for η_3 = 23–33°, and it can then be calculated that the range for τ_c = 33–57°. Wang et al. (2012) reported that the static cutting sliding angle was estimated to be 40–65°. When the friction angle between the vibrating knife and the straw η_3 = 28° and the static cutting sliding angle is 50°, the design requirements for the curve for our cutter are satisfied.

Design of the crank-rocker mechanism for the vibrating knife

The motion of the crank-rocker mechanism in the vibrating knife structure is shown in Fig. 5.

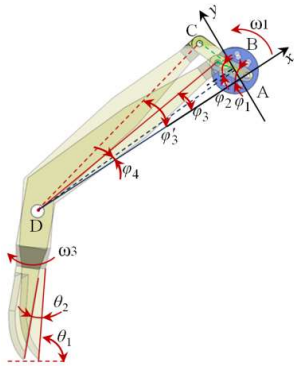

FIGURE 5. Schematic diagram showing the vibration movement of the knife

The crank-rocker mechanism drives the vibrating knife via the connecting rod to achieve reciprocating motion (Mao (2020)). A positional analysis of the crank-rocker mechanism then leads to eqs (15) and (16):

$$\begin{cases} l_1\cos\varphi_1 + l_2\cos\varphi_2 = l_4 + l_3\cos\varphi_3 \\ l_1\sin\varphi_1 + l_2\sin\varphi_2 = l_3\sin\varphi_3 \\ l_{DB} = \sqrt{l_1^{\,2} + l_4^{\,2} - 2l_1l_4\cos\varphi_1} \end{cases} \quad (15)$$

$$\begin{cases} \varphi_2 = \pm\arccos\left(\dfrac{l_2^{\,2} + l_{DB}^{\,2} - l_3^{\,2}}{2l_2l_4}\right) - (\pi - \varphi_4) \\ \varphi_3 = \varphi_4 \pm \arccos\left(\dfrac{l_3^{\,2} + l_4^{\,2} - (l_1 + l_2)^2}{2l_3l_4}\right) \\ \tan\varphi_4 = \dfrac{l_1\sin\varphi_1}{l_1\cos\varphi_1 - l_4} \end{cases} \quad (16)$$

Where:

φ_1 is the angle between segment AB and the x-axis;

φ_2 is the angle between segment CB and the x-axis;

φ_3 is the angle between segment CD and the x-axis when points A, B, and C are collinear but not overlapping;

φ_3' is the angle between segment CD and the x-axis when points A, B, and C are collinear and overlapping;

φ_4 is the angle between segment DB and the x-axis;

ω_1 is the angular velocity of the eccentric wheel;

ω_2 is the angular velocity of rod BC;

ω_3 is the angular velocity of the vibrating knife;

l_1 is the amplification;

l_2 is the length of segment BC;

l_3 is the length of segment CD.

An analysis of the speed of this mechanism yields [eq. (17)]:

$$\begin{cases} \omega_2 = \dfrac{-\omega_1 l_1\sin(\varphi_1 - \varphi_3)}{l_2\sin(\varphi_2 - \varphi_3)} \\ \omega_3 = \dfrac{\omega_1 l_1\sin(\varphi_1 - \varphi 2)}{l_3\sin(\varphi_3 - \varphi_2)} \end{cases} \quad (17)$$

The length of each rod in the crank-rocker mechanism determines the reciprocating trajectory of the vibrating knife. Zhang (2024) found that suitable lengths for the line segments in the crank-rocker mechanism were l_2 = 36 mm, l_3 = 300 mm, and l_4 = 312 mm. Based on the structural nature of the machine tool, the minimum range for the lower limit of l_1 is 10 mm, and the maximum range for the upper limit is 28 mm. To prevent the mechanism from interfering, the range of amplification l_1=14–24 mm. Based on an previous analysis of Figs. 4 and 5, it can be seen that θ_1 affects the trajectory of the vibrating knife and the tangential direction of the edge, which determines the operating effect of the anti-clogging device. However, in order to achieve cutting of the straw, Liu (2021) and Milyutkin et al. (2021) demonstrated that the mounting angle of the vibrating knife must be between 67° and 85°. The mounting angle of the vibrating knife must be θ_1=70–82° in order to avoid collisions between the trajectory of the vibrating knife and the machine tool.

Kinematic analysis of the notched disc and vibrating knife

To explain the anti-clogging mechanism, it is necessary to mechanically analyse the force state during cutting (Wang et al. (2019)). A force analysis of the process of cutting soil with the proposed device is shown in Fig. 6.

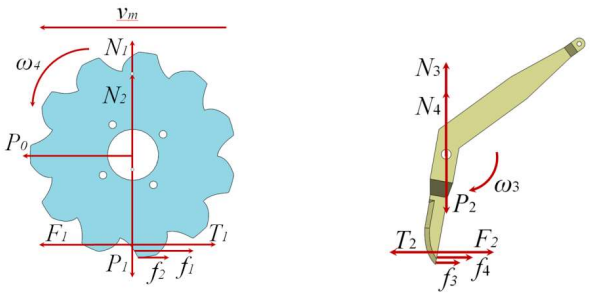

(a) Force analysis of notched disc during the soil cutting process

(b) Force analysis of the vibrating knife during the soil cutting process

FIGURE 6. Force analysis of the process of cutting soil with the notched disc and vibratory knives

Finally, the equilibrium equations for the notched disc can be obtained as given in eqs. (18) and (19):

$$\begin{cases} N_1 + N_2 - P_1 = 0 \\ P_0 + F_1 - T_1 - f_1 - f_2 = 0 \end{cases} \quad (18)$$

$$F_1 = \left(\rho_d g h^2 N_{\rho_d} + chN_c c_a N_{c_a} \right) \quad (19)$$

Where:

N_1 is the supporting force from the soil on the notched disc;

N_2 is the supporting force from the shaft on the notched disc;

P_1 is the downward pressure on the notched disc;

P_0 is the traction force;

F_1 is resistance of the notched disc to cutting the soil;

T_1 is the shearing of soil by the notched disc;

f_1 is the friction force between the notched disc and the soil bottom;

f_2 is the friction force between the side of the notched disc and the soil;

ρ_d is the soil bulk density;

g is the gravitational acceleration;

h is the working depth;

c is the soil cohesion;

c_a is the soil adhesion;

$N\rho_d$, Nc and Nc_a are the soil resistance coefficients for the notched disc.

By combining eqs (18) and (19), the equation for the cutting shear force of the notched disc on the soil can be obtained as [eq. (20)]:

$$T_1 = P_0 + \rho_d g h^2 N_{\rho_d} + chN_c c_a N_{c_a} - \mu_1 \left(P_1 - N_2 \right) - f_2 \quad (20)$$

Where:

μ_1 is the friction coefficient between the notched disc and the soil.

Through the above theoretical analysis, the relevant equations for the vibrating knife can be obtained as shown in eqs (21) and (22):

$$\begin{cases} N_3 + N_4 - P_2 = 0 \\ P_0 + T_2 - F_2 - f_3 - f_4 = 0 \end{cases} \quad (21)$$

$$T_2 = \rho_d g h^2 N'_{\rho_d} + chN'_c c_a N'_{c_a} + f_4 + \mu_2 \left(P_2 - F_4 \right) - P_0 \quad (22)$$

Where:

N_3 is the supporting force from the soil on the vibrating knife;

N_4 is the supporting force from the shaft on the vibrating knife;

P_2 is the downward pressure on the vibrating knife;

T_2 is the shearing of soil by the vibrating knife;

F_2 is resistance of the vibrating knife to cutting the soil;

f_3 is the friction force between the vibrating knife and the soil bottom;

f_4 is the friction force between the side of the vibrating knife and the soil;

$N'\rho_d$, $N'c$ and $N'c_a$ are the soil resistance coefficients of the vibrating knife;

μ_2 is the friction coefficient between the vibrating knife and the soil.

Torque analysis of the notched disc and the vibrating knife

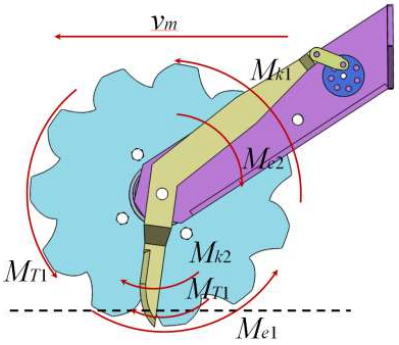

FIGURE 7. Moment analysis of the notched disc and vibrating knife.

As shown in Fig. 7, according to the principle of moment equilibrium, the equation for the analysis of the notched disc cutting tool can be obtained as [eq. (23)].

$$M_{e_1} = M_{T_1} + M_{k_1} \quad (23)$$

Where:

Me_1 is the torque provided by the rack to the notched disc;

M_{T1} is the moment of the notched disc to cut soil;

M_{k1} is the moment of the notched disc to cut straw.

The cutting shear force of the notched disc on the straw (F_{k1}) is given by [eq. (24)], and the cutting shear force of the vibrating knife on the straw (F_{k2}) is given by [eq. (25)]:

$$F_{k_1} = \frac{M_{e_1} - T_1 L_1}{l_5} \tag{24}$$

$$F_{k_2} = \frac{M_{e_2} - T_2 L_2}{l_6} \tag{25}$$

Where:

L_1 is the shear force arm of the notched disc to cut soil;

l_5 is the shear force arm of the notched disc to cut straw;

M_{e2} is the connecting rod providing torque to the vibrating knife;

L_2 is the shear force arm of the vibrating knife to cut soil;

l_6 is the shear force arm of the vibrating knife to cut straw.

Kinematic analysis of disc knives and vibratory knives

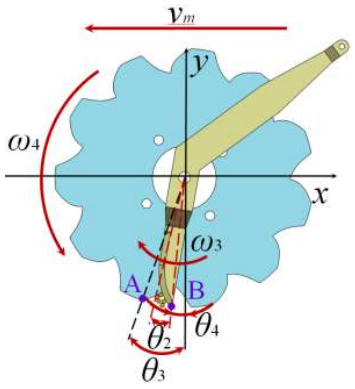

FIGURE 8. Trajectory analysis of the notched disc and vibrating knife.

A kinematic analysis of the anti-clogging device was conducted as shown in Fig. 8. The kinematic equation for point A on the notched disc is given by [eq. (26)], and that for point B is given in [eq. (27)].

$$\begin{cases} x_1 = v_m t - R_2 \sin\left(\theta_3 - \omega_4 t\right) \\ y_1 = R_2 \cos\left(\theta_3 - \omega_4 t\right) \end{cases} \tag{26}$$

Where:

R_2 is the rotation radius of the notched disc;

t is the operating time of the notched disc;

θ_3 is the angle between point A and the negative y-axis;

θ_4 is the angle between point B and the negative y-axis.

$$\begin{cases} \varphi_3{}' - \varphi_3 = \theta_2 = \omega_3 t_0 \\ x_2 = \begin{cases} v_m t + R_3 \sin\left(\theta_4 + \omega_3\left(t - kt_0\right)\right), & \text{k is an odd number} \\ v_m t + R_3 \sin\begin{pmatrix} \theta_4 + \theta_2 \\ -\omega_3\left(t - kt_0\right) \end{pmatrix}, & \text{k is an even number} \end{cases} \\ y_1 = \begin{cases} R_3 \cos\left(\theta_4 + \omega_3\left(t - kt_0\right)\right), & \text{k is an odd number} \\ R_3 \cos\left(\theta_4 + \theta_2 - \omega_3\left(t - kt_0\right)\right), & \text{k is an even number} \end{cases} \end{cases} \tag{27}$$

Where:

t_0 is the time needed for the vibrating knife to move from the initial to the final position;

R_3 is the turning radius of the vibrating knife.

The equation for the notched disc after completing one circular motion is given in [eq. (28)].

$$\begin{cases} \theta_4 + 2k\pi = \theta_4 - \omega_4 \dfrac{l}{v_m} \\ \begin{cases} \theta_5 + 2k\theta_3 = \theta_5 + \omega_3\left(\dfrac{l}{v_m} - kt_0\right), \text{k is an odd number.} \\ \theta_5 + 2k\theta_3 = \theta_5 + \theta_3 - \omega_3\left(\dfrac{l}{v_m} - kt_0\right), \text{k is an even number.} \end{cases} \end{cases} \tag{28}$$

Where:

l is the length of the plot.

From [eq. (28)], it is evident that the rotational speed of the vibrating knife is a crucial parameter of motion that affects the operational performance of the anti-clogging device. Dai et al. (2021) reported that when the forward speed of the machine was set to 6 km/h, the gap between the notched disc and the vibrating knife was 3.5 mm, and the rotational speed range of the vibrating knife was therefore selected as 240–340 rad/min to satisfy the requirements for cutting off the straw.

Experimental setup

The tests were conducted between April 15 and May 15, 2024, using the soil bin experimental setup in the laboratory of Shandong University of Technology. The soil bin had a length of 30 m, a width of 2.8 m, and a depth of 1.8 m, as shown in Fig. 9(b). Prior to the commencement of the experiment, the physical properties of the soil were quantified. The soil water content was found to be 12.6% at a depth of 0–10 cm and 14.3% at a depth of 10–20 cm. The soil compaction was measured as 1.98 MPa at a depth of 10 cm and 2.53 MPa at a depth of 20 cm. The soil bin experiment was designed to simulate actual field conditions, using straw with an average length of 118 mm and an average diameter of 4.2 mm, which was spread uniformly over the soil bin setup with a coverage of 1.1 kg/m².

(a) Support cutting anti-clogging device with vibration for no-till seeder

(b) No-till seeder working diagram

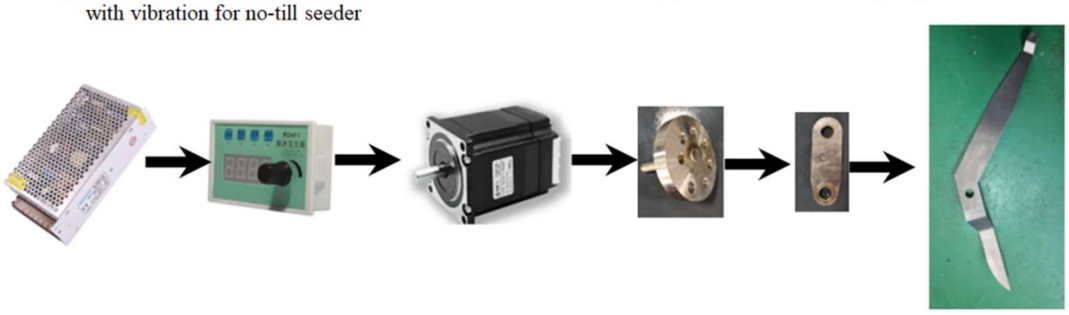

a. Direct current power supply | b. Pulse generator | c. Stepper motor | d. Eccentric wheel | e. Connecting rod | f. Vibrating knife

(c) Motor control system

FIGURE 9. Test site.

The physical setup of the unit is shown in Fig. 9(a). The device was mounted on the no-tillage seeder, which in turn was mounted at the suspension beam position of the dolly, as shown in Fig. 9(b). The height of the frame during the test could be adjusted by the hydraulic system of the trolley to ensure a proper depth of penetration for the implement. The motor control system of the device included a direct current power supply, pulse generator, stepper motor, eccentric wheel, connecting rod, and vibrating knife, as shown in Fig. 9(c). The pulse generator and the stepper motor were powered by a direct current power supply, and the pulse generator regulated the speed of the stepper motor.

The experimental site is shown in Fig. 9(a). The soil tank was divided into three distinct zones: the first 10 m were designated as the acceleration zone, the next 10 m as the deceleration zone, and the last 2 m as the data testing zone. The principal instruments and apparatus used in the test were as follows: a trolley, no-till seeder, the proposed support cutting anti-clogging device, an RCmf-1 pulse generator, a LRS-35-24 transformer direct current power supply, a TDR-300 soil moisture tester, an SC-900 soil tightness meter, a tape measure, a steel plate ruler, and other necessary tools.

Experimental scheme

Parameter optimisation test

The study consisted of three different parts. The first part was a parameter optimisation test that was carried out to investigate the effect of three factors (the mounting angle of the vibrating knife, amplification, and frequency) on the straw cutting rate. Design-Expert software was used to conduct a three-factor, three-level test on the device. The coding results for the factor levels selected for the test are shown in Table 1. The evaluation indexes were the straw cutting rate and the passing ability of the device.

TABLE 1. Factors and levels used in the orthogonal test.

Code	Mounting angle of vibrating knife (°)	Amplification (mm)	Frequency (rad/min)
1	70	14	240
0	76	19	290
−1	82	24	340

Adaptability test

The second part of the test was an adaptability test, in which the adaptability of the straw cutting process was explored at different forward speeds of the machine. The forward speed range of the machine was set to 4–8 km/h, and the optimal parameters from the first part of the test were used to record the test metrics.

Comparison test

The third part was a comparison test, in which the proposed device was compared with an conventional anti-clogging device in terms of the straw cutting rate.

Measurement method

Straw cutting rate

The total number of straws and the number of straws cut were measured during each run of the device. The equation for calculating the straw cutting rate is given by [eq. (29)]:

$$Y = \frac{n_1}{n} \times 100\% \quad (29)$$

Where:

Y is the straw cutting rate;

n is the amount of straw cut by the device;

n_1 is the amount of straw not cut by the device.

Passing ability of the device

The length of the test data collection area was 2 m. Blockage of the implement by straw entanglement in the working area was observed. The soil bin experiment was carried out to assess the adaptability and intended use of the implement according to the relevant documentation.

RESULTS AND DISCUSSION

The test program and results are shown in Table 2. The purposes of this experiment were to establish a mathematical model between the test indicators and evaluation indicators, and to analyse the impact of the test indicators on the evaluation indicators. In this context, X_1, X_2, and X_3 represent the factor coding values.

TABLE 2. Experimental results from a three-factor, three-level orthogonal test.

Serial No.	Experimental factors			Y
	X_1	X_2	X_3	
1	−1	−1	0	92.36
2	1	−1	0	92.62
3	−1	1	0	93.31
4	1	1	0	92.21
5	−1	0	−1	92.12
6	1	0	−1	91.81
7	−1	0	1	93.38
8	1	0	1	92.73
9	0	−1	−1	91.29
10	0	1	−1	91.37
11	0	−1	1	92.41
12	0	1	1	92.71
13	0	0	0	94.72
14	0	0	0	95.11
15	0	0	0	95.27
16	0	0	0	94.86
17	0	0	0	94.64

Variance analysis of experimental results

The test results in Table 2 were analysed by quadratic regression using Design-Expert 13 software, to derive the straw cutting rate. For of each of the factors, the significance and level of influence on the straw cutting rate was analysed and tested in the regression model, as shown in Table 3.

TABLE 3. Variance analysis of experimental results

Source	Sum of squares	Degree of freedom	Mean square	F value	P value
model	30.75	9	3.42	92.93	<0.0001**
X_1	0.6786	1	0.6786	18.46	0.0036
X_2	0.0028	1	0.0028	0.0765	0.7901
X_3	2.81	1	2.81	76.38	<0.0001**
X_1X_2	0.354	1	0.354	9.63	0. 0173
X_1X_3	0.0484	1	0.0484	1.32	0.289
X_2X_3	0.0121	1	0.0121	0.3291	0.5842
X_1^2	4.66	1	4.66	126.67	<0.0001**
X_2^2	11.35	1	11.35	308.64	<0.0001**
X_3^2	8.13	1	8.13	221	<0.0001**
Residual	0.12732	0.2574	7	0.0368	
Loss of fit term	0.0228	0.0561	3	0.0187	0.3714
Pure error	0.10452	0.2013	4	0.0503	
Sum	37.17291	31.01	16		

Note: P ＜0.01;
** means extremely significant

Table 3 reveals that the impact of X_3, X_1^2, X_2^2, and X_3^2 on the straw cutting rate was very significant, while the influence of X_1 and X_1X_2 was also notable. The impact of the other factors was insignificant. The effects of the non-significant items were removed, and variance fitting was performed to produce a multivariate quadratic regression equation for coded values, as shown in [eq. (30)].

$$Y = 94.98 - 0.2913X_1 + 0.0187X_2 + 0.5925X_3 - 0.2975X_1X_2 - 0.11X_1X_3 + 0.055X_2X^3 - 1.05X_1^2 - 1.64X_2^2 - 1.39X_3^2 \quad (30)$$

Surface analysis of experimental results

As shown in Fig. 10, the data were processed using Design-Expert to obtain the response surfaces for the significant interactions between factor effects on the straw cutting rate, and the effect of the three factors on the indicator. Since the tangential force on the blade increases with the installation angle of the vibrating knife, the straw cutting rate initially rises. However, this also reduces the number of straws cut per unit time, which ultimately decreases the cutting rate. Increasing amplification alters the vibrating knife's trajectory and enhances the cutting efficiency, but also results in excessive amounts of straw being cut per unit time, thereby reducing the straw cutting rate. An increase in frequency will result in an increase in the cutting speed of the vibrating blades, thus increasing the straw cutting rate, although this will also lead to an increase in the amount of straw encountered per unit of time, which affects the cutting results.

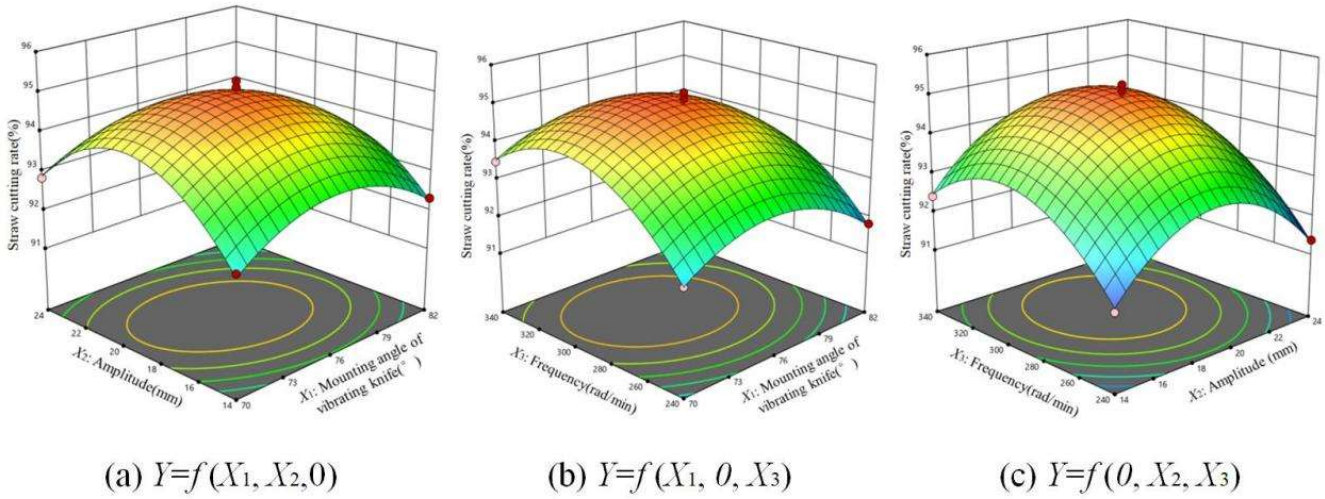

FIGURE 10. Effects of the interaction factors on the straw cutting rate.

As shown in Fig. 10(a), when the amplification is fixed, the straw cutting rate initially increases and then decreases as the initial angle of the mounting angle of vibrating knife is increased, and the behaviour of the curve is the same when the mounting angle of the vibrating knife is fixed. The results shown in this figure have a certain similarity to the experimental results presented by Sun et al. (2015), indicating that the results have a high degree of accuracy. As shown in Fig. 10(b), when the frequency is fixed, the straw cutting rate also tends to increase and then decrease as the mounting angle of vibrating knife increases, and the behaviour of the curve is the same when the mounting angle of the vibrating knife is fixed. As shown in Fig. 10(c), when the frequency is fixed, the straw cutting rate initially increases and then decreases with an increase in amplification, and the behaviour of the curve is the same when the amplification is fixed. The results in this figure show a certain similarity to the experimental results reported by Zhu et al. (2022), indicating that they have a high degree of accuracy.

The experimental data were optimised using Design-Expert software, resulting in the best combination of parameters for the device. When the mounting angle of the vibrating knife was 70.7°, the amplification was 19 mm, and the frequency was 330.2 rad/min, and the straw cutting rate was 94.07%. Three replicated validation tests were carried out using the soil bin experimental setup at Shandong University of Technology. The results were averaged and yielded a straw cutting rate of 94.73%. The validation test showed that the relative error between the measured value and the theoretical value was only 0.66%, thus confirming that this optimal combination can be used as the basis for the parameters of the prototype.

VERIFICATION TESTS

Adaptability test

To assess the adaptability of the device to various forward speeds of the no-till seeder, the straw cutting rate was designated as the evaluation criterion. The forward speed V'_j was varied between 4 and 8 km/h. Through five sets of repetitive tests, the average straw cutting rate Y' was determined as shown in Table 4.

TABLE 4. Experimental results from adaptability and comparison tests.

V_j (km/h)	No.	Y (%)	Y' (%)	Y_t (%)	Y'_t (%)
4	1	92.13	91.18	79.12	79.17
	2	89.65		78.93	
	3	91.76		79.46	
5	1	93.94	93.54	80.85	80.83
	2	92.46		81.23	
	3	94.22		80.41	
6	1	93.78	94.59	81.25	81.03
	2	94.54		80.53	
	3	95.46		81.31	
7	1	94.35	94.10	81.64	81.22
	2	93.76		81.43	
	3	94.21		80.59	
8	1	93.76	93.10	79.78	80.14
	2	92.89		80.52	
	3	92.68		80.12	
Average	-	-	93.30	-	80.48

As can be seen from Table 4, as the forward speed of the no-till seeder increases, the straw cutting rate initially increases and then decreases, with a relatively smooth trend. The reason for this variation is that an increase in the forward speed of the machine leads to an increase in the cutting speed of the notched disc, thus increasing the straw cutting rate. However, if the forward speed exceeds a critical value, it will lead to an increase in the amount of straw per unit of time, thus leading to a decrease in the straw cutting rate. This change is attributed to the direct relationship between the forward speed and the cutting efficiency of the machine, which influences its overall performance in terms of straw cutting and cleaning operations. The results showed that the average straw cutting rate was 93.30%. In summary, the straw cutting rate of the no-till seeder within this speed range can meet the operational requirements, and the device can adapt to different operational speeds and environments.

Comparison test

Several replicated tests were conducted on conventional notched discs under the same conditions to determine the average straw cutting rate Y'_t. The results in Table 4 indicate that when the proposed support cutting anti-clogging device with vibration was used with the no-till seeder, the straw cutting rate was 12.82% higher compared to a traditional anti-clogging device. These findings demonstrate that the anti-clogging device developed in this study significantly outperformed the traditional version.

CONCLUSIONS

(1) To solve the problem in which straw often winds around the working parts of a no-tillage seeder, a support

cutting anti-clogging device with vibration was designed. This device overcomes the challenges associated with the extensive areas and full straw coverage involved in no-till planting operations.

(2) A mechanical model of straw cutting was established to reveal the anti-blocking mechanism. The main structural parameters of the device were determined through theoretical calculations and kinematic analysis, with a value for the mounting angle of the vibrating knife of θ_1 = 70–82°, an amplification of l_1=14–24 mm, and a frequency of ω_m = 240–340 rad/min.

(3) A soil bin experiment was conducted to elucidate the effects of each of the three factors, and Design-Expert software was used to construct regression models for the three factors associated with each indicator. The optimal structural parameters derived were as follows: mounting angle for the vibrating knife θ_1 = 70.7°, amplification l_1 = 19 mm, and frequency ω_m = 330.2 rad/min. At these values, the straw cutting rate was 94.07%. The relative error between the measured and theoretical values after the validation test was only 0.66%, thus demonstrating the reliability of the data.

(4) The results of an adaptability test indicated that the device was capable of performing effectively at various operating speeds, with an average straw cutting rate of 93.30%. Furthermore, the results of a comparative test demonstrated the device's superior efficiency in regard to cutting straw in clogging environments. All performance indices surpassed those of a traditional anti-clogging device, with the average straw cutting rate showing an improvement of 12.82%.

ACKNOWLEDGEMENTS

The authors are grateful to Shandong Province Youth Innovation Team Development Plan of Universities (2022KJ225), the National Key Research and Development Program of China (Grant No. 2021YFD2000401), the Opening Fund of the State Key Laboratory of Agricultural Equipment Technology (Grant No. NKL-2023-010), and the High Quality Development Project of the Ministry of Industry and Information Technology of China (Grant No. 2023ZY02009)

REFERENCES

Bi, S. Y., Liu, W. D., & Guo, L. J. (2020). Simulation analysis and optimization test of structural parameters of stubble cutting. *Journal of Agricultural Mechanization Research*, 42(07), 172–179. https://doi.org/10.13427/j.cnki.njyi.2020.07.028

Chen, H. T., Zha, S. H., Dun, G. Q., Cong, G. B., Li, A., & Feng, Y. N. (2016). Optimization and experiment of cleaning device of 2BMF type no-till precision seeder. *Transactions of the Chinese Society for Agricultural Machinery*, 47(07), 96–102. https://doi.org/10.6041/j.issn.1000-1298.2016.07.014

Dai, Y. S., Jia, H. J., Xiong, Y., Liu, B. Y., Cheng, X., & Wong, L. C. (2021). Impact of conservation tillage measures on maize yield, soil organic carbon and nitrogen components of maize field in rain-fed region in southwest China. *Agricultural Research in the Arid Areas*, 39(03), 82–90. https://doi.org/10.7606/j.issn.1000-7601.2021.03.10

Fallahi, S., & Raoufat, M. (2007). Row-crop seeder attachments in a conservation tillage system: A comparative study. *Soil Tillage Research*, 98(1), 27–34. https://doi.org/10.1016/j.still.2007.10.005

Fan, X. H., Jia, H. L., Zhang, W. H., Yang, H. T., & Gu, Y. Q. (2011). Parametric analysis of finger-type anti-blocking residue-cleaner for no-till planting. *Transactions of the Chinese Society for Agricultural Machinery*, 42(10), 56–60. https://doi.org/10.3969/j.issn.1000-1298(2011).10-0056-05

Hong, Y. (2021). *The design and research of weed divider blocking device in no tillage seeder*. (Master's thesis, University of Science and Technology). https://doi.org/10.27200/d.cnki.gkmlu.2021.000313

Huang, Y. X., Gao, P. Y., Zhang, Q. K., Shen, H., Zhu, R. X., & Shi, J. T. (2020). Design and experiment of grass-soil separation device with combination of stubble cutting and grass guiding used for no-till seeder. *Transactions of the Chinese Society for Agricultural Machinery*, 51(05), 67–78. https://doi.org/10.6041/j.issn.1000-1298.2020.05.007

Li, Y. X., Lu, C. Y., Li, H. W., He, J., Wang, Q. J., Huang, S. H., Gao, Z., Yuan, P. P., Wei, X. Y., & Zhan, H. M. (2022). Design and experiment of spiral discharge anti-blocking and row-sorting device of wheat no-till seeder. *Agriculture*, 12(4), 468–468. https://doi.org/10.3390/AGRICULTURE12040468

Liao, Q. X., Xie, H. M., Zhang, Q. S., Zhang, J. Q., Ao, Q., & Wang, L. (2023). Design and experiment of driven disc plow and double-edged rotary tillage combined tiller. *Transactions of the Chinese Society for Agricultural Machinery*, 54(07), 99–110+195. https://doi.org/10.6041/j.issn.1000-1298.2023.07.010

Liu, H. (2021). Design and experimental research of axial low-frequency vibration. *Journal of Xi'an Shiyou University (Social Science Edition)*. https://doi.org/10.27400/d.cnki.gxasc.2021.000329

Liu, Z. P., Tian, M., Yang, S. X., & He, R. Y. (2018). Design of a grass separation equipment with driven rotating tooth disk. *Journal of South China Agricultural University*, 39(01), 120–124. https://doi.org/10.7671/j.issn.1001-411X.2018.01.019

Mao, L. (2020). *Anti-blocking device for a field channel* (in patent application approval process; USPTO 20200056345). https://www.freepatentsonline.com/y2020/0056345.html

Milyutkin, V., Zhiltsov, S., Guzhin, I., Sazonov, D., & Artamonov, E. (2021). *Feasibility demonstration of the effective design of the opener group of the seeder for winter wheat in arid conditions*. BIO Web of Conferences, 37, 00120. https://doi.org/10.1051/BIOCONF/20213700120

Sun, W. T., Lv, Y. M., & Li, Q. (2015). Influence on vibratory bowl feeder with different leaf spring angle. *Light Industry Machinery*, 33(04), 12–15+19. https://doi.org/10.3969/j.issn.1005-2895.2015.04.003

Wang, H. Y., Chen, H. T., & Ji, W. Y. (2012). Anti-blocking mechanism of type 2BMFJ-3 no-till precision seeder for wheat stubble fields. *Transactions of the Chinese Society for Agricultural Machinery*, 44(04), 64–70. https://doi.org/10.6041/j.issn.1000-1298.2013.04.012

Wang, X., Qi, J. Y., Jing, Z. H., Li, C., & Zhang, H. L. (2019). Effects of long-term conservation tillage on soil aggregate stability and carbon and nitrogen in paddy field. *Transactions of the Chinese Society of Agricultural Engineering (CSAE)*, 35(24), 121–128. https://doi.org/10.11975/j.issn.1002-6819.2019.24.015

Yao, W. Y., Zhao, D. B., Xu, G. F., Chen, M. Z., Miao, H. Q., & Diao, P. S. (2020). Design and experiment of anti-blocking device for strip to row active corn no-tillage seeding. *Transactions of the Chinese Society for Agricultural Machinery*, 51(S2), 55–62+71. https://doi.org/10.6041/j.issn.1000-1298.2020.S2.007

Yao, W. Y., Zhao, D. B., Miao, H. Q., Cui, P. D., Wei, M. J., & Diao, P. S. (2022) Design and experiment of oblique anti-blocking device for no-tillage seeder with shallow plowing stubble clearing. *Transactions of the Chinese Society for Agricultural Machinery*, 53(08), 42–52. https://doi.org/10.6041/j.issn.1000-1298.2022.08.005

Zhang, J. (2024). Analysis and applying of MATLAB-based optimization design method for crank rocker mechanism. *Mechanical and Electrical* Information, 03, 36–38. https://doi.org/10.19514/j.cnki.cn32-1628/tm.2024.03.009

Zhang, Y. P., Du, R. C., Diao, P. S., Yang, S. D., & Wang, W. Z. (2017). Design and experiment of wide band seeding rice seeder with reversed stubble cleaning and anti-blocking. *Transactions of the Chinese Society of Agricultural Engineering (CSAE)*, 33(03), 7–13. https://doi.org/10.11975/i.issn.1002-6819.2017.03.002

Zhao, H. B., He, J., Li, H. W., Liu, C.G., Zheng, K., & Zhang, Z. Q. (2018). Design and experiment of strip rotary-cut-throw anti-blocking implement. *Transactions of the Chinese Society for Agricultural Machinery*, 49(05), 65–75. https://doi.org/10.6041/j.issn.1000-1298.2018.05.008

Zhu, H. B., Qian, C., Bai, L. Z., Zhao, H. R., Ma, S. A., Zhang, X., & Li, H. (2022). Design and experiments of active anti-blocking device with forward-reverse rotation. *Transactions of the Chinese Society of Agricultural Engineering (Transactions of the CSAE)*, 38(01), 1–11. https://doi.org/10.11975/j.issn.1002-6819.2022.01.001

Zhu, H. B., Zhang, X., Hong, Y., Bai, L. Z., & Zhao, H. R. (2023). Design and experiment of bionic shifting and diffluence straw anti-blocking device. *Agricultural Research in the Arid Areas*, 41(04), 318–328. https://doi.org/10.7606/j.issn.1000-7601.2023.04.33